Feasibility Analysis of Reduced-Scale Visual Corona Tests in High Voltage Laboratories

Carlos Abomailek [1], Jordi-Roger Riba [1*], and Pau Casals-Torrens [1]

[1] Electrical Engineering Department, Universitat Politècnica de Catalunya, AMBER Laboratory, Campus Terrassa – Zona IPCT Ctra Nac. 150 km 14, 08227 Terrassa, Spain
[*] riba@ee.upc.edu

Abstract: Corona is a critical effect that must be considered during the design and optimization stages of high-voltage hardware such as substation connectors, since due to the harmful effects, corona threats power systems reliability. Visual corona tests allow detecting and identifying the critical corona points on the surface of substation connectors, so corrective actions can be applied for product optimization. This paper focuses on reduced-scale visual corona tests intended to verify and optimize the behaviour of such high-voltage hardware. Reduced-scale visual corona tests allow reducing the voltage to be applied, laboratory size, instrumentation requirements, assembly and test times, and finally the overall costs of the tests compared to standard corona tests carried out in large-size high-voltage laboratories. A hybrid approach combining experimental tests and finite element method (FEM) simulations is presented, which allows obtaining the equivalent visual corona onset voltage between reduced-scale and full-scale tests. Although the paper focuses on the analysis of aluminium substation connectors, the proposed approach can be applied to many other hardware intended for high-voltage applications.

1. Introduction

Although substation connectors are simple devices, they play a crucial role in electrical substations. Substation connectors interconnect the different elements of the facility [1], and thus, a suitable and optimized design is highly desirable. Substation connectors must pass different standard tests to ensure a suitable performance (thermal, mechanical, corrosion, or electromagnetic) under nominal operating conditions [2]. Before undergoing compulsory standard tests, the new designed connectors are extensively validated in the laboratory to ensure appropriate performance and reliability, especially when mathematical models are not available. Extensive experimental tests of full-scale prototypes presents some drawbacks, such as added complexity [3], extended assembling and test time [4], and consequently high cost [5] [6]. Downscale or reduced-scale (RS) modelling and testing allows partially overcoming the abovementioned drawbacks, since this approach offers a simpler and cost-effective solution, which has been successfully applied in different areas such as aeronautics [7], [8], aerodynamics [9], mechanical [10] and electrical engineering [11] or heat transfer [4], [12] among others. The design of reduced-scale tests has been greatly facilitated by the emergence of powerful computers and software [4], which currently have a deep impact on design capabilities and procedures. Reduced-scale models are nowadays considered as viable, valuable and essential design tools [7]. However, when deriving equivalences between reduced- and full-scale (FS) prototypes, it has to be ensured that reduced-scale prototypes fully characterize the full-scale object [11]. In the electrical engineering area, reduced-scale modelling and testing has been applied in several applications including research in micro grids [13], overvoltage in power transformer windings [3], GIS (gas-insulated switchgear) [5], or the study of corona and breakdown conditions in high-voltage applications using test cages [11], [14], [15] , among others.

Full-scale standard corona tests of high-voltage hardware often require large-size fully screened laboratories with extra high-voltage capability [16] which are very scarce, so the tests result very expensive [17]. This often forces industry to conduct standard corona tests in external high-voltage laboratories, where the customer habitually has to face long waiting times. The employees of the external laboratory carry out the standard corona tests, with virtually no intervention of the customer's engineers and, thus, the customer does not acquire important information and experience regarding the performance of the analysed high-voltage products or about possible product improvements.

Reduced-scale models allows speeding up and reducing the cost of corona tests, because the high-voltage generator and complementary accessories required to perform these tests are more affordable that those required in large-size high-voltage laboratories. The size of the test hall and the mandatory clearances are also drastically reduced, these being critical factors that severely limit to carry out routinely corona tests in factory laboratories.

When performing correctly-designed reduced-scale corona tests at a reduce voltage level, the electric field distribution nearby the test object follows the same pattern than that resulting in the full-scale test [11], [18] at higher voltages. Comparative studies between reduced- and full-scale tests analysing the electromagnetic behaviour of dc and ac power lines have been widely reported in the technical literature [19]–[21]. In [12] it is stated that when analysing full- and reduced-scale models, the ion current density, electric field distribution, and corona activity of monopolar dc and single-phase ac lines, exhibit a great similarity.

Corona discharges produce undesired effects such as audible noise, electromagnetic interference, ozone, or power loss among others [22]–[25]. According to several international standards [26], [27], high-voltage hardware must be virtually free of corona for the specified conditions of operation.

Visual corona tests are advantageous since they allow identifying the critical points regarding corona appearance. The information acquired from visual corona tests is very useful, since a precise assessment of the corona onset conditions plays a key role to design devices intended for high-voltage applications [22], [24], [28]. Visual corona tests are conducted in darkened laboratories, since most of the corona radiation falls within the ultraviolet spectrum, thus being almost imperceptible in daylight to the human eye [29].

This paper analyses the feasibility of conducting reduced-scale visual corona tests for product optimization in unscreened industrial laboratories with a limited voltage output. This solution is appealing since it allows a drastic reduction of the requirements of the high-voltage generator and a consequent size reduction of the testing area, since the test voltage can be reduced and the generator does not require being free of partial discharges. A DSLR (digital single-lens reflex) camera can be used to detect corona activity [30], [31], so the requirements of the corona measuring instruments are also reduced, whereas assembly and testing times and thus the overall costs of the tests are also reduced. In addition, the design engineers can perform the corona tests in the manufacturer's facilities, thus avoiding to face long waiting times to conduct such tests in external laboratories, while also collecting many useful product information and experience about corona behaviour, he same product engineers can perform the tests. This strategy also allows optimizing the connector in case it does not fulfil the requirements dictated by the standards.

This paper applies three-dimensional FEM (3D-FEM) simulations to determine the surface voltage gradient of the reduced- and full-scale connectors, similarly as done in [11], [32]. The proposed approach also locates the critical corona points of the connector's surface. FEM simulations are well-suited to this end [11], [33], since they allow analysing accurately full- and reduced-scale tests with reasonable time of simulation. This was corroborated by the work of Hu et al. [32], who deduced equivalences between reduced- and full-scale models of bundle conductors from the information gathered by means of FEM simulations. However, there is a lack of works performing a detailed analysis of the corona onset voltage for complex shaped three-dimensional downscale high-voltage hardware. However, downscaled models are highly appealing since when combined with FEM simulations, allow analysing corona onset conditions economically and accurately and deriving relationships to infer the behaviour of full-scale prototypes.

This paper also proposes a method based on the Peek's law to determine the equivalence between the visual corona onset voltage for reduced-scale and full-scale tests.

The visual corona tests proposed in this work are very advantageous since they allow locating by means of experiments the most stressed areas and points of the connector when the electrical stress of the connector is pushed to its limits. The approach proposed in this work allows testing the connector under operating conditions even severer than those found in real environments, and thus a safety margin can be settled for design purposes. The usefulness and accuracy of the proposed method is validated by means of visual corona tests carried out on different connectors, which are downsized by a scale factor 1:1.745. The methodology presented in this paper can be applied to diverse high-voltage hardware, including conductors, corona protections, or fittings for substation and power lines among others.

2. The analysed substation connectors

This paper deals with 5 models of A356 aluminium substation connectors, from the catalogue of SBI Connectors, two of which have been manufactured at two scales, that is, FS (full scale, 1:1) and RS (reduced scale, 1:1.745), which are shown in Fig. 1.

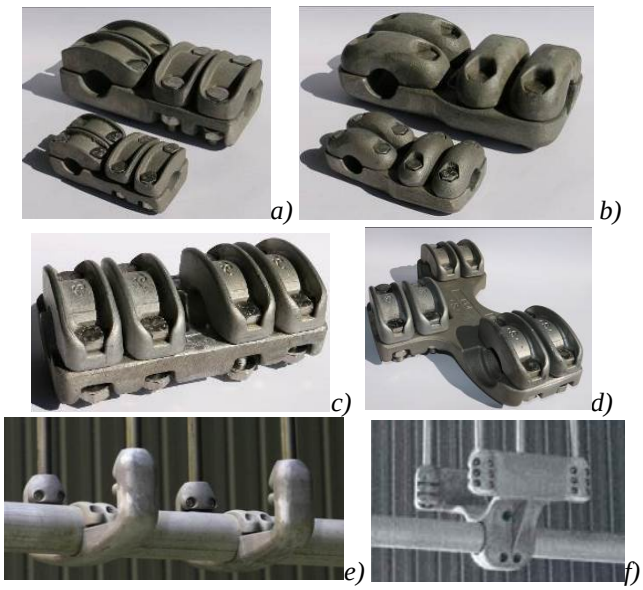

Fig. 1. *The five models of substation connectors analysed in this paper. a) T-type connector J285TLS, FS and RS with a scale factor 1:1.745. b) T-type connector S285TLS, FS and RS with a scale factor 1:1.745. c) Coupler connector J40S33PK. d) Double coupler connector J40S33DPK. e) Duplex T-type connector Z12T390D9DLSP. f) Quadruplex T-type connector Z390Q9T12DNS.*

Table 1 shows the main features of the conductors or bus bars at which each analysed substation connector are linked.

Table 1 Conductors associated to each connector

Connector designation	Scale	Conductor 1	Conductor 2
J285TLS	FS	GTACSR-464 (ϕ = 27.6 mm)	GTACSR-464 (ϕ = 27.6 mm)
J285TLS	RS	GTACSR-131/19 (ϕ = 15.79 mm)	GTACSR-131/19 (ϕ = 15.79 mm)
S285TLS	FS	GTACSR-464 (ϕ = 27.6 mm)	GTACSR-464 (ϕ = 27.6 mm)
S285TLS	RS	GTACSR-131/19 (ϕ = 15.79 mm)	GTACSR-131/19 (ϕ = 15.79 mm)
J40S33PK	FS	Al bus bar (ϕ = 33 mm)	Al bus bar (ϕ = 40 mm)
J40S33DPK	FS	Al bus bar (ϕ = 33 mm)	Al bus bar (ϕ = 40 mm)
Z12T390D9DLSP	FS	Al bus bar (ϕ = 120 mm)	Quad bundle Al rod (ϕ = 39 mm)
Z390Q9T12DNS	FS	Al bus bar (ϕ = 120 mm)	Quad bundle Al rod (ϕ = 39 mm)

It is noted that the reduced scale factor is the ratio between the physical dimensions of the original connector

and the reduced scale version. This ratio is mainly restricted by the availability of conductors and the metrics of screws and nuts. Both FS and RS versions of the connectors have to fit in commercially-available conductors. The second restriction is related to the metrics of the screws and nuts. Whereas the metrics of the bolting elements in the FS connectors is M10, the RS ones use M6 metrics. As a result, the connectors have a scale relationship of 1:1.745.

3. The approach proposed in this paper

This section details the approach proposed in this work to perform reduced scale visual corona tests intended for product optimization, in a small-size unscreened high-voltage laboratory, which typically can be located at the facilities of the manufacturer. This approach allows drastically reducing the requirements in terms of maximum voltage, nominal power, laboratory size, instrumentation or assembly and testing times with respect to those required in full-scale corona tests, thus speeding up the optimal design process and experimental validation of the prototypes.

Fig. 2 shows the approach proposed in this paper. The first step, as shown in Fig. 2, is related to the experimental analysis and FEM simulation of the reduced-scale connector. Step 1 consists of several stages as follows,

- Step 1.1. The RS connector is assembled in the high-voltage laboratory to conduct the visual corona test.
- Step 1.2. The visual corona test is performed and long exposure photographs are taken to detect corona activity. The visual corona extinction voltage is determined.
- Step 1.3. The corona onset points on the surface of the connector are located.
- Step 1.4. The surface voltage gradient in the corona points located in step 1.3 is calculated by means of FEM simulations when applying the visual corona extinction voltage obtained in step 1.2.
- The second step is related to the FEM simulation of the full-scale connector. This step consists of the following steps,
- Step 2.1. The corrected curvature radius of the FS connector is calculated by applying (5).
- Step 2.2. Locate the corona onset points on the surface of the connector. These points are the equivalent points of the RS connector located in step 1.3.
- Step 2.3. Calculate the surface voltage gradient at the corona points of the FS connector located in step 2.2, by applying (6).
- Step 2.4. By simulating through FEM the geometry of the FS connector when placed at the standard height above ground plane, calculate the test voltage V_{FS} to be applied, at which the surface voltage gradient in the corona points located in step 2.2 is that calculated in step 2.3.

The test object must be free of visual corona activity at the acceptance test voltage [34], so it passes the visual corona test when the visual extinction voltage is greater than the specified one. Finally, if the voltage V_{FS} calculated in step 2.4 is higher than the acceptance test voltage, the FS connector will pass the standard corona test, otherwise the geometry of the connector must be revised in order to obtain an improved design. In this latter case, once le geometry has been improved, start again from step 1.1.

The strategy summarized in Fig. 2 can be applied during the optimal design stage of substation connectors and many other high-voltage components, since it ensures that the final design will pass the mandatory standard corona test.

This paper assumes that it is feasible to conduct corona tests at a reduced height above the ground plane, since under corona inception conditions, the locations of the most stressed points and the electric field strength in such locations, are virtually not influenced by the height of the connector. More details about this hypothesis can be found in [25].

4. FEM simulations

Corona inception occurs when the surface electric field strength surpasses the critical inception value, so air molecules are ionized due to collisions with electrons, thus evolving into an electron avalanche discharge. Although it is possible to analyse the corona effect by means of simulations, due to complexity involved in the electro-chemical reactions and the computational requirements, most works deal with very simple geometries [35], [36]. The complex molecular reactions occurring within the air during the discharge are not simulated in this paper, since it focused to determine the surface electric field strength before corona appearance, so that the corona inception condition can be determined from experimental measurements.

The approach presented in Fig. 2 is based on experimental visual corona tests and three-dimensional FEM (3D-FEM) simulations performed with the Comsol Multiphysics® software [37]. Such simulations are applied to determine the surface voltage gradient in the points of the connectors generating corona, since no effective sensors are available for this purpose. Both the experimental visual corona onset voltage and the geometry of the experimental RS test are introduced in the FEM software, from which the critical corona points (those susceptible of corona appearance) of the connector surface are located and the surface voltage gradient in these points is calculated.

The surface voltage gradient in the surface points of the connector is determined from the Poisson's equation [38],

$$\vec{\nabla}\cdot\vec{E} = \rho / \varepsilon \tag{1}$$

E (V/m) being the voltage gradient, ρ (C/m3) the charge density, and ε (F/m) the permittivity of the region under study, which is assumed as a constant. By applying $\vec{E} = -\vec{\nabla}\cdot U$, where U (V) is the scalar electrical potential, (1) leads to the Poisson's equation for electrostatics, which allows calculating the electrical potential and thus the voltage gradient in the points of interest,

$$\nabla^2 U = -\rho/\varepsilon \tag{2}$$

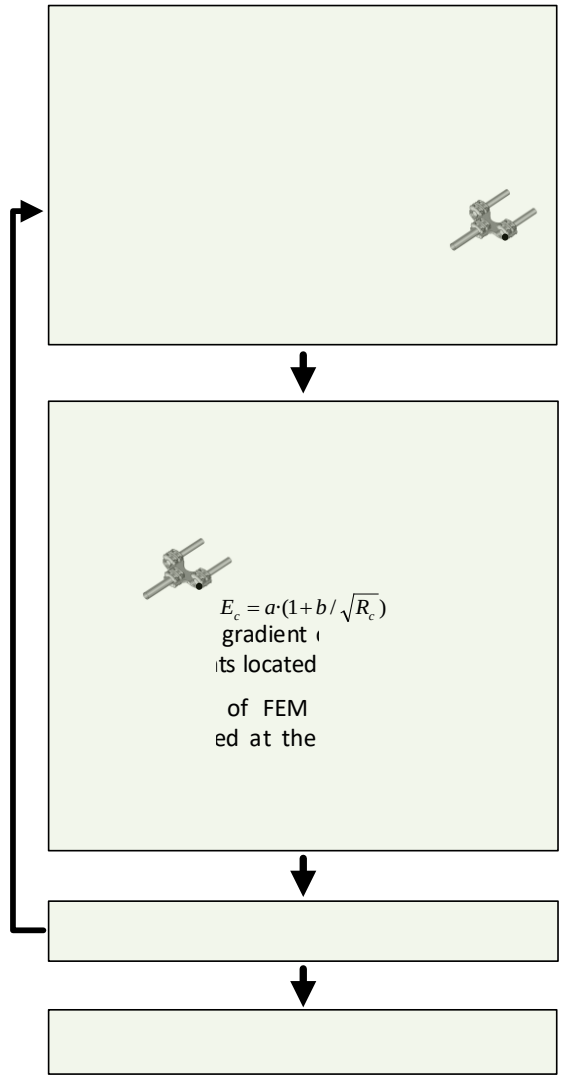

Fig. 2. *Summary of the approach proposed in this work.*

Fig. 3 shows the meshes of some of the eight types of substation connectors analysed in this work.

5. Experimental visual corona tests

Visual corona tests were carried out in the AMBER high-voltage laboratory of the Universitat Politècnica de Catalunya using a calibrated 130 kV BK-130 high-voltage generator from Phenix technologies. Fig. 4 shows the layout used to carry out this test.

The visual corona was detected by using a Canon EOS-70D digital camera. It includes a 20.2 Mpixels CMOS APS-C sensor (22.5 mm x 15 mm). The corona onset points on the surface of the tested connectors were located with the high-voltage laboratory completely darkened by means of large exposure photographs (1 minute) to increase the number of photons converted into electrical signals by the CMOS sensor. The results presented in this paper are based on the visual corona extinction voltage, since it is lower than the corona inception voltage. The corona extinction voltage is found by gradually reducing the applied voltage from above the corona inception voltage [39].

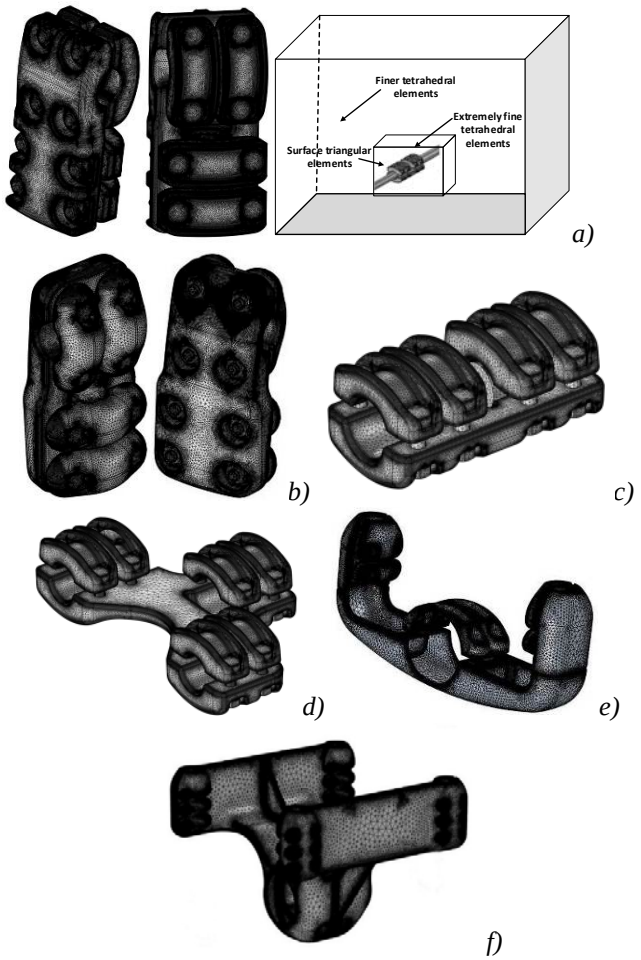

Fig. 3. Some of the analysed substation connectors. Geometry and meshes applied in the FEM simulations. a) T-type connector J285TLS, FS, RS and simulation domain. b) T-type connector S285TLS, FS and RS. c) Coupler connector J40S33PK. d) Double coupler connector J40S33DPK. e) Duplex T-type connector Z12T390D9DLSP. f) Quadruplex T-type connector Z390Q9T12DNS.

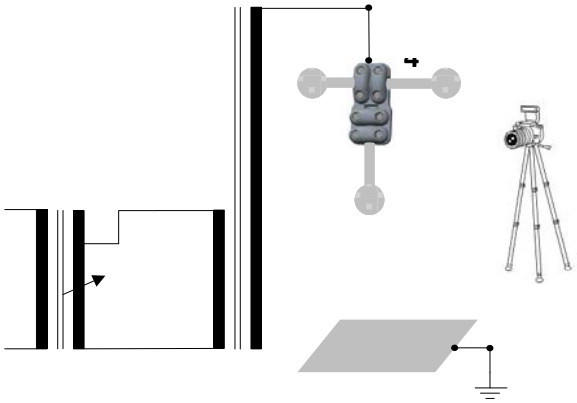

Fig. 4. *High-voltage generator used for the experimental tests.*

Since the corona extinction voltage is influenced by the local atmospheric conditions [28], experimental values found in the laboratory must be corrected to take into account this effect. Therefore, this paper transforms the measured voltages under local atmospheric conditions to the standard atmosphere (101.3 kPa, 20 ºC, and absolute humidity 11 g/m^3) by applying the method proposed in in the IEEE Std 4-2013 standard [40].

Although negative alternating current (50 Hz) corona appears first than positive corona for air gaps larger than 20 mm, visual corona photographs were taken during positive corona occurrence according to the IEEE Std 1829-2017 [34] standard. To determine the visual corona extinction voltage, the following procedure suggested in the IEEE Std 1829-2017 was applied,

1.- Increase the voltage gradually and slowly until observing positive corona on the surface of the connector under test. This is the corona inception voltage.
2.- Next, the voltage is increased by 10% and maintained for 60 seconds.
3.- Finally, the voltage is lowered slowly until observing the extinction of positive corona. This is the positive corona extinction voltage.

Steps 1 to 3 where repeated 3 times for each connector and the average value was calculated. A photographic report was also performed.

Fig. 5 shows the corona discharges at the corona critical points of the eight substation connectors analysed in this paper photographed and located by the digital camera.

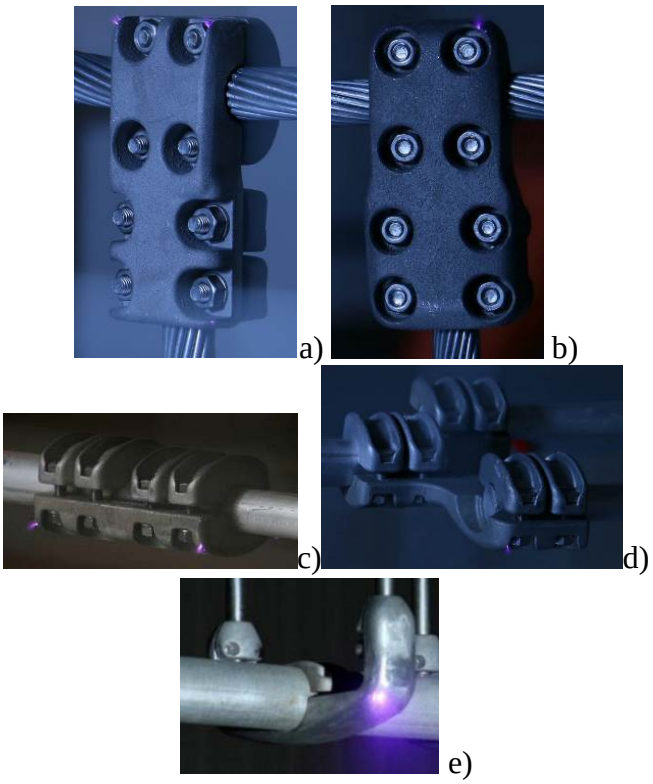

Fig. 5. *Visual positive corona photographs taken with the digital camera of the different models of substation connectors analyzed in this paper. a) T-type connector J285TLS. b) T-type connector S285TLS. c) Coupler connector J40S33PK. d) Double coupler connector J40S33DPK. e) Duplex T-type connector Z12T390D9DLSP.*

Table 2 summarizes the results obtained in this section. It shows the corrected positive visual extinction voltage of all analysed connectors. These results are the basis to calculate the corona surface voltage gradient on the critical corona points and to obtain a mathematical law relating the surface voltage gradient in the points of the reduced scale connector during corona onset conditions and the surface voltage gradient of the full scale connector.

Table 2 Visual corona tests. Positive corona extinction voltage and height above ground level

Connector reference	Corrected extinction voltage (kV_{RMS})*	Height above ground (m)
J285TLS (FS)	105.9	1.05
J285TLS (RS)	68.7	0.60
S285TLS(FS)	133.4	1.05
S285TLS(RS)	91.9	0.60
J40S33PK	98.0	0.32
J40S33DPK	101.0	0.45
Z12T390D9DLS	663.0	6.00
Z390Q9T12DNS	558.0	5.00

*Corrected to standard atmospheric conditions [40].

6. Experimental and FEM results

As detailed in Section 3, the surface voltage gradient during visual corona occurrence can be obtained by means of 3D-FEM simulations once the corona extinction voltage has been determined from the experimental visual corona tests carried out by means of the digital camera, which allows identifying the critical corona points on the surface of the test object. This section performs FEM simulations of each connector, which replicate the same geometry and boundary conditions as in the experimental corona tests. It is noted that the voltage applied in such simulations is the positive corona extinction voltage obtained from the visual corona tests. By applying such strategy, the surface voltage gradient on the corona critical points of the connector is obtained as shown in Fig. 6.

In the case of cylinders or conductors, Peek's law relates the surface voltage gradient during visual corona inception conditions with the curvature radius of the conductor [17], [41]–[46]. According to Peek's law, the visual corona surface inception voltage gradient E_c (kV_{peak}/cm) at power frequency (50/60 Hz) for an isolated round conductor, two parallel conductors or coaxial cylinders of radius r (cm) can expressed as,

$$E_c = E_o \cdot m \cdot \delta \left(1 + a / \sqrt{\delta \cdot r}\right) \quad (3)$$

E_o (kV_{peak}/cm) being the disruptive visual voltage gradient measured at standard atmospheric conditions, m a surface roughness factor and δ the relative air density. When dealing with standard atmospheric conditions the relative air density is unity. It is noted that at power frequency E_o takes values around 30-31 kV_{peak}/cm and a around 0.301-0.308 $cm^{1/2}$ depending on the specific conductor configuration. Note that the general form of (3) can be rewritten as,

$$E_c = b \cdot \left(1 + c / \sqrt{r}\right) \quad (4)$$

where b (kV_{peak}/cm) and c ($cm^{1/2}$) are parameters, whose values depend on the specific geometry of the problem. In this work, (4) is applied to determine a relationship between the visual corona surface inception voltage gradient and the curvature radius of the critical corona points. It is noted that

Fig. 7 plots the surface voltage gradient versus the curvature radius of the critical corona points of eight models of connectors. The curvature radius was obtained from the CAD of each connector. The visual corona extinction voltage of the eight connectors was obtained from visual corona tests carried on in the high-voltage laboratory. Next, the surface voltage gradient at the corona critical points was obtained by

means of FEM simulations. Therefore, the information presented in Fig. 7 combines experimental and simulation results.

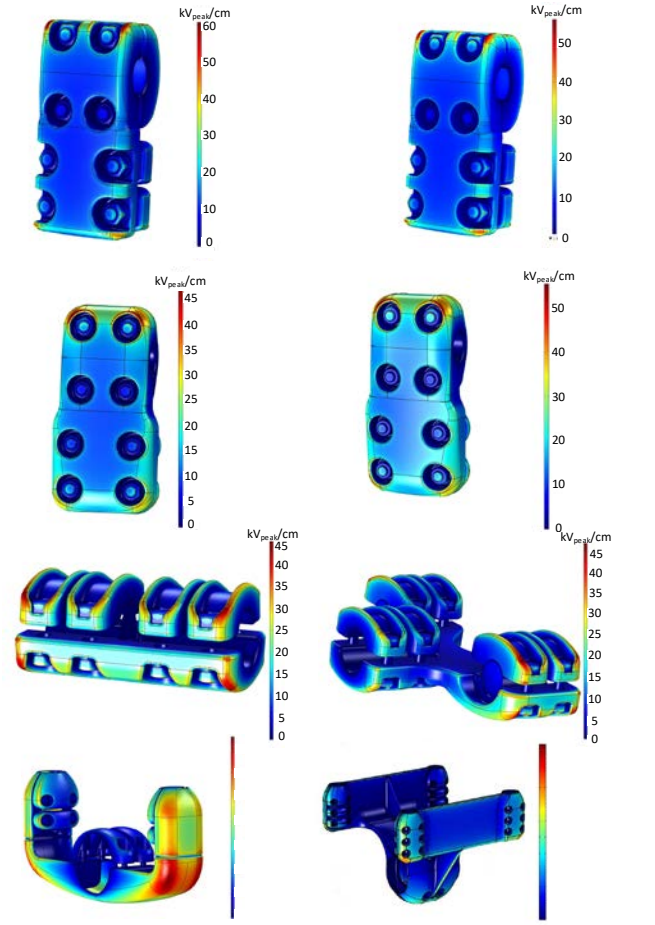

Fig. 6. *Surface voltage gradient obtained by means of FEM simulations, highlighting the critical corona points. a) T-type connector J285TLS (FS and RS). b) T-type connector S285TLS (FS and RS). c) Coupler connector J40S33PK. d) Double coupler connector J40S33DPK. e) Duplex T-type connector Z12T390D9DLSP. f) Quadruplex T-type connector Z390Q9T12DNS.Arreglar figura I escala*

The clouds of points (R_{corona_point},E_c) characterizing the connectors in Fig. 7, represent the neighbouring points around the critical corona point on the surface of such connector, since it is never a discrete single point. However, results presented in Fig. 7 do not show a good agreement with (4). This is attributed to the fact that instead of the curvature radius of the corona critical points, it is better to deal with the corrected curvature radius R_c (cm), which is calculated as,

$$R_c = R_{corona\_point} \cdot \frac{D_{corona\_point}}{R_{conductor}} \qquad (5)$$

R_{corona_point} (cm) being the curvature radius of the corona inception point, D_{corona_point} (cm) the distance between the corona inception point and the symmetry axis of the connector (see Fig. 8a) and $R_{conductor}$ (cm) the radius of the reference conductor. Note that (5) is an equivalent or effective radius that takes into account not only the curvature radius of the critical corona point, but also the radius of the conductor and the outer radius of the connector, as shown in Fig. 8a. The transformation in (5) makes sense since the connector dimensions increase with the radius of the conductor. When D_{corona_point} and $R_{conductor}$ increase, the surface voltage gradient at the connector surface tends to decrease. This is effect is similar to the effect of bundled conductors in power lines as an effective means to increase the effective radius and reduce the surface voltage gradient at the conductors for a given applied voltage. Therefore, instead of (4), this paper proposes to apply,

$$E_c = b \cdot (1 + c / \sqrt{R_c}) \qquad (6)$$

where E_c (kV_{peak}/cm) is expressed by assuming standard atmospheric conditions, so there is no need to include the relative air density δ in (6).

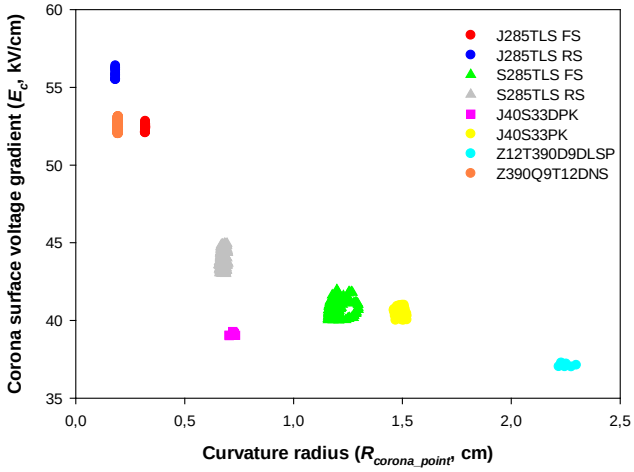

Fig. 7. *Peak value of the visual corona voltage gradient versus the curvature radius of the critical corona points at the connector surface. FS stands for full scale, whereas RS stands for reduced scale.*

Table 3 summarizes the values of the parameters in (5) for all the connectors analysed in this paper.

Table 3 Parameters in (5)

Connector reference	R_{corona_point} **(mm)**	D_{corona_point} **(mm)**	$R_{conductor}$ **(mm)**	r^* **(-)**
J285TLS (FS)	3.1922	42.8	13.8	3.10
J285TLS (RS)	1.8197	24.5	7.9	3.11
S285TLS(FS)	11.9687	46.0	13.8	3.33
S285TLS(RS)	6.7507	26.3	7.9	3.34
J40S33PK	14.9976	46.7	16.5	2.83
J40S33DPK	7.1904	141.2	16.5	8.56
Z12T390D9DLS	22.5078	252.5	60	4.21
Z390Q9T12DNS	1.9451	253.7	60	4.17

* $r = D_{corona\_point}/R_{conductor}$

Fig. 8b shows the surface voltage gradient versus the corrected curvature radius of the critical corona points of the eight models of connectors dealt with, as well as the fitting of (6). The fitting has been done by taking into account the central points of each cloud of points, which correspond to the critical corona points of each connector.

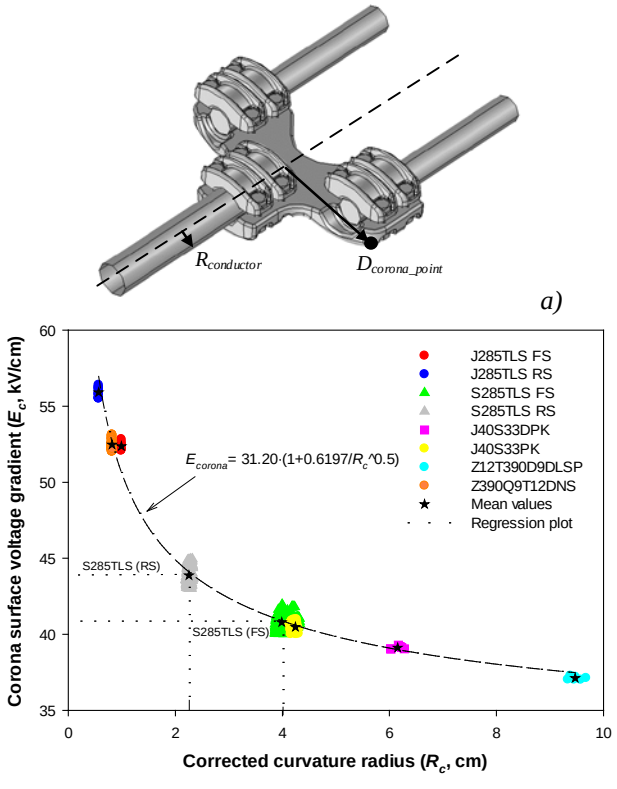

Fig. 8. *a) Connector and the parameters $R_{conductor}$ and D_{corona_point} to calculate the corrected curvature radius R_c. b) Peak value of the visual corona surface voltage gradient versus the corrected curvature radius of the critical corona points at the connector surface.*

Table 4 summarizes the parameters resulting from the least squares fitting of (6) from the experimental/simulation data shown in Fig. 8b.

Table 4 Fitting of $E_c = b\cdot(1 + c/\sqrt{R_c})$ (6)

Parameter	Value
b (kV_{peak}/cm)	31.20 (29.50, 32.89)[1]
c ($cm^{1/2}$)	0.6197 (0.5209, 0.7185)[1]
R-square[2]	0.9883
Adjusted R-square[2]	0.9863
SSE (sum of squares due to error)[2]	4.269
RMSE (root mean squared error)[2]	0.8435

[1] 95% confidence bounds
[2] Goodness of fit statistics

The results presented in Fig. 8b and Table 4 clearly show a good match between experimental/simulated results and (6). Therefore, (6) can be applied to determine the visual corona surface gradient and the visual corona onset voltage (from FEM simulations) of the FS connector once those of the RS connector have been obtained from a reduced-scale visual corona test. It is noted that the obtained value of parameter b (31.20 kV_{peak}/cm) is very close to that proposed by Peek for polished round conductors (30-31 kV_{peak}/cm depending on the specific geometry).

The paper has also proved that (6) is almost independent of the height of the tested connector above ground plane, since the results presented in this paper are based on heights between 0.32 and 6 m. It is worth noting that the height reduction during industrial tests allows an important decrease of both the corona onset voltage and a great reduction of assembling and test times.

7. Conclusion

Standard corona tests intended for substation connectors and other high-voltage components, require very specific high-voltage facilities, are time-consuming and costly. This work has proposed a reduced-scale approach for speeding up, simplifying and reducing the cost of visual corona tests designed to validate and optimize the behavior of substation connectors. The proposed approach combines reduced-scale experimental corona tests performed with a digital camera to locate the corona critical points and 3D-FEM simulations. Eight substation connectors have been tested in different laboratories and analyzed through 3D-FEM simulations to validate experimentally the hypothesis formulated. An equation based on Peek's law has been proposed to determine the visual corona surface gradient, and thus the visual corona onset voltage obtained from FEM simulations, of the FS connector once those of the RS connector have been obtained from visual corona tests. The experimental/simulation results presented in this paper have proved the accuracy and feasibility of the proposed reduced-scale approach, thus validating the proposed equation to relate RS with FS corona tests. These encouraging results suggest that reduced-scale testing and simulation can be an essential tool to assess the corona performance of substation connectors and other high-voltage components for power lines and electrical substations, while allowing to reduce development costs of new products.

8. Acknowledgments

The authors would like to thank SBI-Connectors Spain that supported this study by provisioning the samples and the equipment required for the experimental tests. They also thank the Spanish Ministry of Economy and Competitiveness for the financial support received under contract RTC-2014-2862-3. The authors also wish to acknowledge the financial support from the Generalitat de Catalunya (GRC MCIA, Grant nº 2017 SGR 967).

9. References

[1] F. Capelli, J.-R. Riba, and J. Pérez, "Three-Dimensional Finite-Element Analysis of the Short-Time and Peak Withstand Current Tests in Substation Connectors," *Energies*, vol. 9, no. 6, p. 418, May 2016.

[2] C. Abomailek, F. Capelli, J.-R. Riba, and P. Casals-Torrens, "Transient thermal modelling of substation connectors by means of dimensionality reduction," *Appl. Therm. Eng.*, vol. 111, pp. 562–572, 2017.

[3] Q. Yang, Y. Chen, W. Sima, and H. Zhao, "Measurement and analysis of transient overvoltage distribution in transformer windings based on reduced-scale model," *Electr. Power Syst. Res.*, vol. 140, pp. 70–77, 2016.

[4] C. P. Coutinho, A. J. Baptista, and J. Dias Rodrigues, "Reduced scale models based on similitude theory: A review up to 2015," *Eng. Struct.*, vol. 119, pp. 81–94, 2016.

[5] H. Li, N. Shu, X. Wu, H. Peng, and Z. Li, "Scale Modeling on the Overheat Failure of Bus Contacts in Gas-Insulated Switchgears," *IEEE Trans. Magn.*, vol. 50, no. 2, pp. 305–308, Feb. 2014.

[6] R. G. Urban, H. C. Reader, and J. P. Holtzhausen, "Small Corona Cage for Wideband HVac Radio Noise Studies: Rationale and Critical Design," *IEEE Trans. Power Deliv.*, vol. 23, no. 2, pp. 1150–1157, Apr. 2008.

[7] Joseph Chambers, *Modeling Flight : The role of dynamically scale*. NASA, 2015.

[8] S. Lebental, K. C. Hall, D. B. Bliss, J. Dolbow, L. E. Howle, and J. Protz,

"Optimization of the aerodynamics of small-scale flapping aircraft in Hover," Duke University, 2008.

[9] F. Meinert *et al.*, "A Correlation Study of Wind Tunnels for Reduced-Scale Automotive Aerodynamic Development," *SAE Int. J. Passeng. Cars - Mech. Syst.*, vol. 9, no. 2, pp. 2016-01-1598, Apr. 2016.

[10] A. A. Alnaqi, D. C. Barton, and P. C. Brooks, "Reduced scale thermal characterization of automotive disc brake," *Appl. Therm. Eng.*, vol. 75, pp. 658–668, 2015.

[11] J. Hernandez-Guiteras, J. R. Riba, P. Casals-Torrens, and R. Bosch, "Feasibility analysis of reduced-scale air breakdown tests in high voltage laboratories combined with the use of scaled test cages," *IEEE Trans. Dielectr. Electr. Insul.*, vol. 20, pp. 1590–1597, 2013.

[12] S. Rabe and B. Schartel, "The rapid mass calorimeter: Understanding reduced-scale fire test results," *Polym. Test.*, vol. 57, pp. 165–174, 2017.

[13] S. D. Sudhoff *et al.*, "A reduced scale naval DC microgrid to support electric ship research and development," in *2015 IEEE Electric Ship Technologies Symposium (ESTS)*, 2015, pp. 464–471.

[14] F.-C. Lu, S.-H. You, Y.-P. Liu, Q.-F. Wan, and Z.-B. Zhao, "AC Conductors' Corona-Loss Calculation and Analysis in Corona Cage," *IEEE Trans. Power Deliv.*, vol. 27, no. 2, pp. 877–885, Apr. 2012.

[15] S. A. Sebo, D. G. Kasten, T. Zhao, L. E. Zaffanella, B. A. Clairmont, and S. Zelingher, "Development of reduced-scale line modeling for the study of hybrid corona," in *Proceedings of IEEE Conference on Electrical Insulation and Dielectric Phenomena - (CEIDP '93)*, pp. 538–543.

[16] X. Bian *et al.*, "Corona-generated space charge effects on electric field distribution for an indoor corona cage and a monopolar test line," *IEEE Trans. Dielectr. Electr. Insul.*, vol. 18, no. 5, pp. 1767–1778, Oct. 2011.

[17] M. S. Naidu and V. Kamaraju, *High Voltage Engineering*. New York: Tata McGraw-Hill Publishing Company Limited, 1996.

[18] Y. Nakano and Y. Sunaga, "Availability of corona cage for predicting audible noise generated from HVDC transmission line," *IEEE Trans. Power Deliv.*, vol. 4, no. 2, pp. 1422–1431, Apr. 1989.

[19] L. Xie, L. Zhao, J. Lu, X. Cui, and Y. Ju, "Altitude Correction of Radio Interference of HVDC Transmission Lines Part I: Converting Method of Measured Data," *IEEE Trans. Electromagn. Compat.*, vol. 59, no. 1, pp. 275–283, Feb. 2017.

[20] L. Zhao, X. Cui, L. Xie, J. Lu, K. He, and Y. Ju, "Altitude Correction of Radio Interference of HVdc Transmission Lines Part II: Measured Data Analysis and Altitude Correction," *IEEE Trans. Electromagn. Compat.*, vol. 59, no. 1, pp. 284–292, Feb. 2017.

[21] F. Yin, M. Farzaneh, and X. Jiang, "Corona investigation of an energized conductor under various weather conditions," *IEEE Trans. Dielectr. Electr. Insul.*, vol. 24, no. 1, pp. 462–470, Feb. 2017.

[22] C. Zhang, Y. Yi, and L. Wang, "Positive dc corona inception on dielectric-coated stranded conductors in air," *IET Sci. Meas. Technol.*, vol. 10, no. 6, pp. 557–563, Sep. 2016.

[23] J. Hernández-Guiteras, J.-R. Riba, and P. Casals-Torrens, "Determination of the corona inception voltage in an extra high voltage substation connector," *IEEE Trans. Dielectr. Electr. Insul.*, vol. 20, no. 1, pp. 82–88, Feb. 2013.

[24] Z.-X. Li, J.-B. Fan, Y. Yin, and G. Chen, "Numerical calculation of the negative onset corona voltage of high-voltage direct current bare overhead transmission conductors," *IET Gener. Transm. Distrib.*, vol. 4, no. 9, p. 1009, 2010.

[25] J.-R. Riba, C. Abomailek, P. Casals-Torrens, and F. Capelli, "Simplification and cost reduction of visual corona tests," *IET Gener. Transm. Distrib.*, vol. 12, no. 4, pp. 834–841, Feb. 2018.

[26] ANSI/NEMA, "ANSI/NEMA CC1. Electric Power Connection for Substation." Rosslyn, Virginia, 2009.

[27] International Electrotechnical Commission, *IEC 60270:2000 High-voltage test techniques - Partial discharge measurements*, 3.0. International Electrotechnical Commission, 2000.

[28] Z. Qiu, J. Ruan, D. Huang, S. Shu, and Z. Du, "Prediction study on positive DC corona onset voltage of rod-plane air gaps and its application to the design of valve hall fittings," *IET Gener. Transm. Distrib.*, vol. 10, no. 7, pp. 1519–1526, May 2016.

[29] A. L. Souza and I. J. S. Lopes, "Experimental investigation of corona onset in contaminated polymer surfaces," *IEEE Trans. Dielectr. Electr. Insul.*, vol. 22, no. 2, pp. 1321–1331, Apr. 2015.

[30] D. S. Prasad and B. S. Reddy, "Digital image processing techniques for estimating power released from the corona discharges," *IEEE Trans. Dielectr. Electr. Insul.*, vol. 24, no. 1, pp. 75–82, Feb. 2017.

[31] D. S. Prasad and B. S. Reddy, "Study of corona degradation of polymeric insulating samples using high dynamic range imaging technique," *IEEE Trans. Dielectr. Electr. Insul.*, vol. 24, no. 2, pp. 1169–1177, Apr. 2017.

[32] Q. Hu, L. Shu, X. Jiang, C. Sun, S. Zhang, and Y. Shang, "Effects of air pressure and humidity on the corona onset voltage of bundle conductors," *IET Gener. Transm. Distrib.*, vol. 5, no. 6, p. 621, Jun. 2011.

[33] F. Yang, P. Cheng, H. Luo, Y. Yang, H. Liu, and K. Kang, "3-D thermal analysis and contact resistance evaluation of power cable joint," *Appl. Therm. Eng.*, vol. 93, pp. 1183–1192, Jan. 2016.

[34] IEEE, "IEEE Std 1829-2017 - IEEE Guide for Conducting Corona Tests on Hardware for Overhead Transmission Lines and Substations," 2017.

[35] J. Jadidian, M. Zahn, N. Lavesson, O. Widlund, and K. Borg, "Effects of Impulse Voltage Polarity, Peak Amplitude, and Rise Time on Streamers Initiated From a Needle Electrode in Transformer Oil," *IEEE Trans. Plasma Sci.*, vol. 40, no. 3, pp. 909–918, Mar. 2012.

[36] P. Dordizadeh, K. Adamiak, and G. S. Peter Castle, "Numerical investigation of the formation of Trichel pulses in a needle-plane geometry," *J. Phys. D. Appl. Phys.*, vol. 48, no. 41, p. 415203, Oct. 2015.

[37] Comsol, "COMSOL 4.3 Multiphysics User's Guide." COMSOL, p. 1292, 2012.

[38] J. Hernández-Guiteras, J.-R. Riba, and L. Romeral, "Redesign process of a 765kVRMS AC substation connector by means of 3D-FEM simulations," *Simul. Model. Pract. Theory*, vol. 42, pp. 1–11, 2014.

[39] IEEE, "IEEE Std 100-2000 The Authoritative Dictionary of IEEE Standards Terms, Seventh Edition," *IEEE Std 100-2000*. pp. 1–1362, 2000.

[40] IEEE, "IEEE Std 4-2013 (Revision of IEEE Std 4-1995) IEEE Standard for High-Voltage Testing Techniques," *IEEE Std 4-2013 (Revision of IEEE Std 4-1995)*. pp. 1–213, 2013.

[41] The Central Station Engineers of The Westinghouse Eectric and Corporation, *Electrical Transmission and Distribution Reference Book*, Fourth edi. East Pittsburgh, Pennsylvania: Westinghouse, 1964.

[42] Electric Power Research Institute, *Transmission line reference book 345 kV and above*, 2014 Editi. Palo Alto, CA: Electric Power Research Institute (EPRI), 2014.

[43] Cigré Working Group 36.01, "ADDENDUM to CIGRE Document N° 20 (1974) : INTERFERENCES PRODUCED BY CORONA EFFECT OF ELECTRIC SYSTEMS," 1974.

[44] A. Carsimamovic, A. Mujezinovic, S. Carsimamovic, Z. Bajramovic, M. Kosarac, and K. Stankovic, "Calculation of the corona onset voltage gradient under variable atmospheric correction factors," in *IEEE EUROCON 2015 - International Conference on Computer as a Tool (EUROCON)*, 2015, pp. 1–5.

[45] A. Fridman, A. Fridman, and L. A. Kennedy, *Plasma Physics and Engineering*, Second Edi. CRC Press, 2011.

[46] F. W. Peek, "The Law of Corona and the Dielectric Strength of Air-II," *Proc. Am. Inst. Electr. Eng.*, vol. XXXI, no. 7, pp. 1051–1092, Jul. 1911.